Neuron, Vol. 29, 681–690, March, 2001, Copyright ©2001 by Cell Press

Calcium Dependence of Exocytosis and Endocytosis at the Cochlear Inner Hair Cell Afferent Synapse

Dirk Beutner,*†‡ Thomas Voets,* Erwin Neher,* and Tobias Moser*†
*Department of Membrane Biophysics
Max-Planck-Institute for Biophysical Chemistry
Am Fassberg
37077 Göttingen
†Department of Otolaryngology
Göttingen University Medical School
Robert-Koch-Strasse
37073 Göttingen
Germany

Summary

Release of neurotransmitter at the inner hair cell (IHC) afferent synapse is a fundamental step in translating sound into auditory nerve excitation. To study the Ca^{2+} dependence of the underlying vesicle fusion and subsequent endocytosis, we combined Ca^{2+} uncaging with membrane capacitance measurements in mouse IHCs. Rapid elevations in $[Ca^{2+}]_i$ above 8 μM caused a biphasic capacitance increase corresponding to the fusion of $\sim$40,000 vesicles. The kinetics of exocytosis displayed a fifth-order Ca^{2+} dependence reaching maximal rates of $>3 \times 10^7$ vesicle/s. Exocytosis was always followed by slow, compensatory endocytosis ($\tau \approx 15$ s). Higher $[Ca^{2+}]_i$ increased the contribution of a faster mode of endocytosis with a Ca^{2+}-independent time constant of $\sim$300 ms. These properties provide for rapid and sustained transmitter release from this large presynaptic terminal.

Introduction

Cochlear inner hair cells transduce mechanical stimuli into receptor potentials, which in turn control the release of neurotransmitter onto postsynaptic receptors of the auditory nerve (for review, see Sewell, 1996). Their specialized role in translating sound into auditory nerve stimulation sets high demands on the synaptic transmission at the IHC active zones. First, mammalian IHCs must be able to transmit timing information about sound signals with frequencies of up to 2 kHz (e.g., Kiang et al., 1965). This extraordinary performance requires very rapid release of synaptic vesicles. Second, IHCs can maintain transmitter release, albeit at reduced rates, in response to sustained sound stimuli that last for hours (Kiang et al., 1965). This implies that IHCs either contain a virtually inexhaustible pool of releasable vesicles or possess a very efficient mechanism of vesicle recruitment.

Like many other sensory cells (e.g., retinal bipolar cells, electroreceptors, photoreceptors, or taste buds), IHCs contain ribbon-type active zones (Smith and Sjostrand, 1961). The synaptic ribbons are plate-like, proteinasceous structures packed with synaptic vesicles and anchored to the presynaptic density. It has often been suggested that the ability of sensory cells to produce both rapid and sustained phases of neurotransmitter release originates from these specialized ribbon structures (Parsons et al., 1994; von Gersdorff et al., 1996). In this view, the fast phasic release corresponds to the fusion of release-ready vesicles attached to the membrane at the bottom of the ribbon close to Ca^{2+} channels, whereas the slower sustained release reflects the downward movement of vesicles from the upper rows of the ribbon to the release sites and their subsequent fusion. In agreement herewith are functional studies showing that goldfish retinal bipolar cells and mouse IHCs contain a small vesicle pool that can be readily released by short stimuli and rapidly refills (Mennerick and Matthews, 1996; Gomis et al., 1999; Moser and Beutner, 2000). Moreover, the size of this pool in bipolar cells corresponds well to the number of vesicles docked to the membrane at the bottom of the ribbons, as determined by electron microscopy (von Gersdorff et al., 1996). However, synaptic vesicles are not strictly confined to the ribbons in these cell types, and results from total internal reflection fluorescence microscopy (TIRFM) experiments performed in goldfish retinal bipolar neurons show the occurrence of release events away from the ribbon-type active zones (Zenisek et al., 2000). Therefore, it is likely that sustained release originates, at least partially, from the exocytosis of fusion competent vesicles distal from the ribbon structures. The slower release of these vesicles could then simply reflect the lower $[Ca^{2+}]_i$ signal that these vesicles experience due to the longer distance from Ca^{2+} channels.

The use of flash photolysis of caged Ca^{2+} to create spatially homogenous increases in $[Ca^{2+}]_i$ has proved to be a powerful method to determine the number of fusion competent vesicles and their release kinetics independent of their localization to Ca^{2+} channels. Interestingly, Ca^{2+} concentrations of 20–100 μM are needed to drive exocytosis in goldfish bipolar ribbon synapses (Heidelberger et al., 1994), whereas submicromolar to low micromolar concentrations already cause robust release at fast central synapses (Bollmann et al., 2000; Schneggenburger and Neher, 2000) as well as in neuroendocrine cells (Heinemann et al., 1994; Voets, 2000). This difference led to the suggestion that low Ca^{2+} affinity exocytosis is a hallmark of sustained neurotransmitter release at ribbon synapses preventing a too rapid exhaustion of releasable vesicles at moderate Ca^{2+} concentrations (Matthews, 2000). However, it is not clear whether the lower Ca^{2+} affinity observed in the bipolar cell preparation from goldfish retina can be generalized to mammalian ribbon-type active zones.

Here, we combined flash photolysis of caged Ca^{2+} and high time resolution whole-cell measurements of membrane capacitance (C_m) to study the Ca^{2+}-dependent kinetics of exocytosis and endocytosis in mouse cochlear IHCs. On average, a total pool of about 40,000 fusion competent vesicles was released in two kinetically distinct phases. The steep Ca^{2+} dependence of

‡To whom correspondence should be addressed (e-mail: dbeutne@gwdg.de).

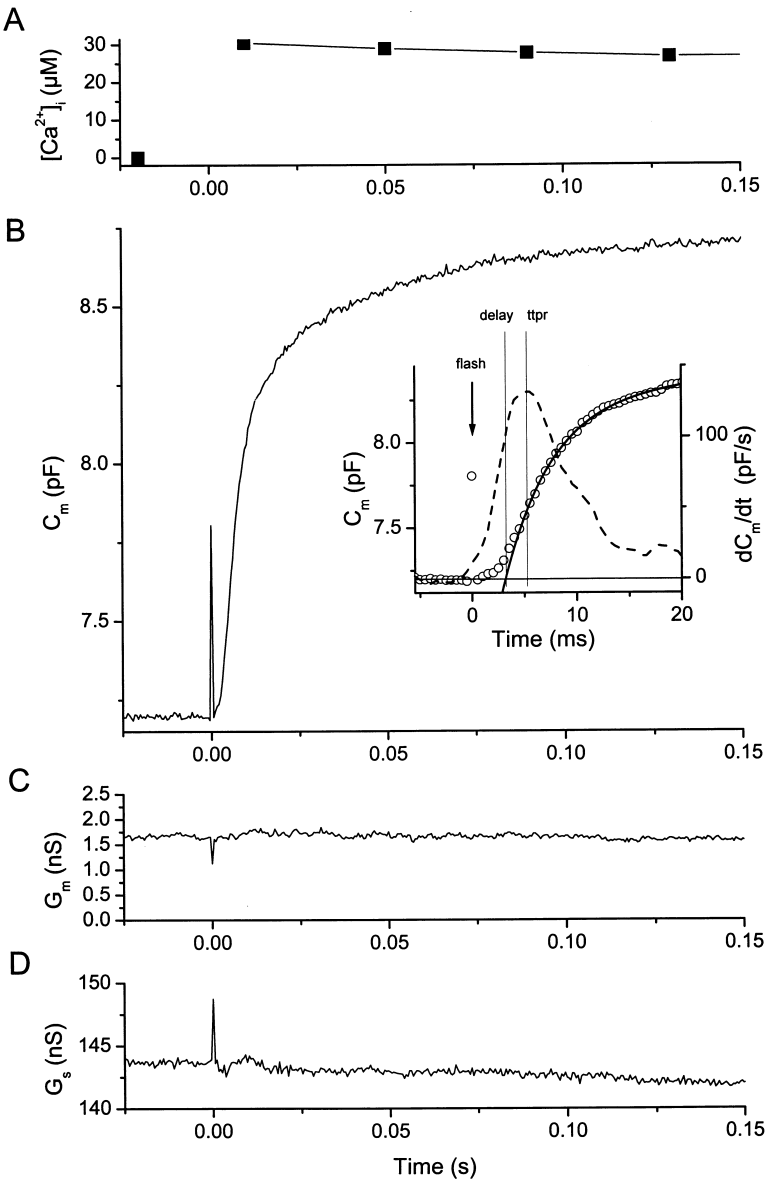

Figure 1. Exocytosis in Response to Flash Photolysis of Ca^{2+}-Loaded DM-Nitrophen

(A) Ratiometric measurement of $[Ca^{2+}]_i$ using the calcium indicator dye furaptra. $[Ca^{2+}]_i$ values were estimated from the ratio of the fluorescence signals measured during 15 ms illuminations at 350 and 380 nm. Before the flash, $[Ca^{2+}]_i$ was too low to be accurately measured with this low affinity dye.

(B) Recording of membrane capacitance (C_m) in response to a UV flash. The flash was given at time = 0, indicated by the flash artifact in all lock-in estimates. The inset shows the first 20 ms after the flash on an expanded time scale. The C_m response (circles) was well fitted by a double exponential function with time constants of 5.3 and 57 ms, respectively (superimposed line). The dashed line represents the first time derivative of the C_m trace (dC_m/dt). The time to peak release (ttpr, 5.1ms) was estimated as the time difference between flash and the peak of dC_m/dt. The exocytic delay (2.8 ms) was calculated from the time difference between the flash and the x axis crossing of the back-extrapolated double-exponential fit to the C_m data. From the exocytic delay and the ttpr, 0.4 ms were subtracted to account for the delay introduced by the flash time course and the time required for calcium to be released from photolyzed DM-nitrophen.

(C and D) Lack of changes in membrane conductance (G_m) or series conductance (G_s) after the flash.

the fast secretory component is described with a kinetic model incorporating five Ca^{2+} binding steps preceding an irreversible fusion reaction. Simulation of the rate of exocytosis during depolarization showed that Ca^{2+} at release sites does not need to exceed values of around 30 μM in order to account for the observed fusion kinetics of the readily releasable vesicle population (~300 vesicles, see Moser and Beutner, 2000). Two distinct mechanisms of endocytosis followed flash-induced secretion. Ca^{2+} triggered the faster mode of endocytosis but did not affect its time course.

Results

Exocytosis in Response to Flash Photolysis of Caged Ca^{2+}

In this study, IHCs were dialyzed in the whole-cell patch-clamp configuration (Hamill et al., 1981) with a pipette solution containing the photolabile Ca^{2+} cage DM-nitrophen (Kaplan and Ellis-Davies, 1988) and the Ca^{2+} indicator Furaptra (Konishi et al., 1991). Before flash photolysis, $[Ca^{2+}]_i$ was generally too low to be accurately measured by the low-affinity dye furaptra. Cellular Mg^{2+} is known to compete with and displace Ca^{2+} when Ca^{2+}-loaded DM-nitrophen enters into cells, which can result in a transient elevation of $[Ca^{2+}]_i$ and a secretory response in neuroendocrine cells (Neher and Zucker, 1993). However, we did not observe such loading transients in C_m and/or $[Ca^{2+}]_i$, probably reflecting the effective Ca^{2+} clearance mechanisms of IHCs.

After equilibration of cage and Ca^{2+} indicator with the cytoplasm, exocytosis was triggered by a brief flash of UV light that liberated Ca^{2+} from its cage and resulted in a stepwise increase in $[Ca^{2+}]_i$. Figure 1 displays a typical experiment where uncaging resulted in an increase of $[Ca^{2+}]_i$ to 30 μM (Figure 1A). The sudden rise in $[Ca^{2+}]_i$ caused a rapid, biphasic increase in C_m of about 1.5 pF that saturated within 150 ms (Figure 1B).

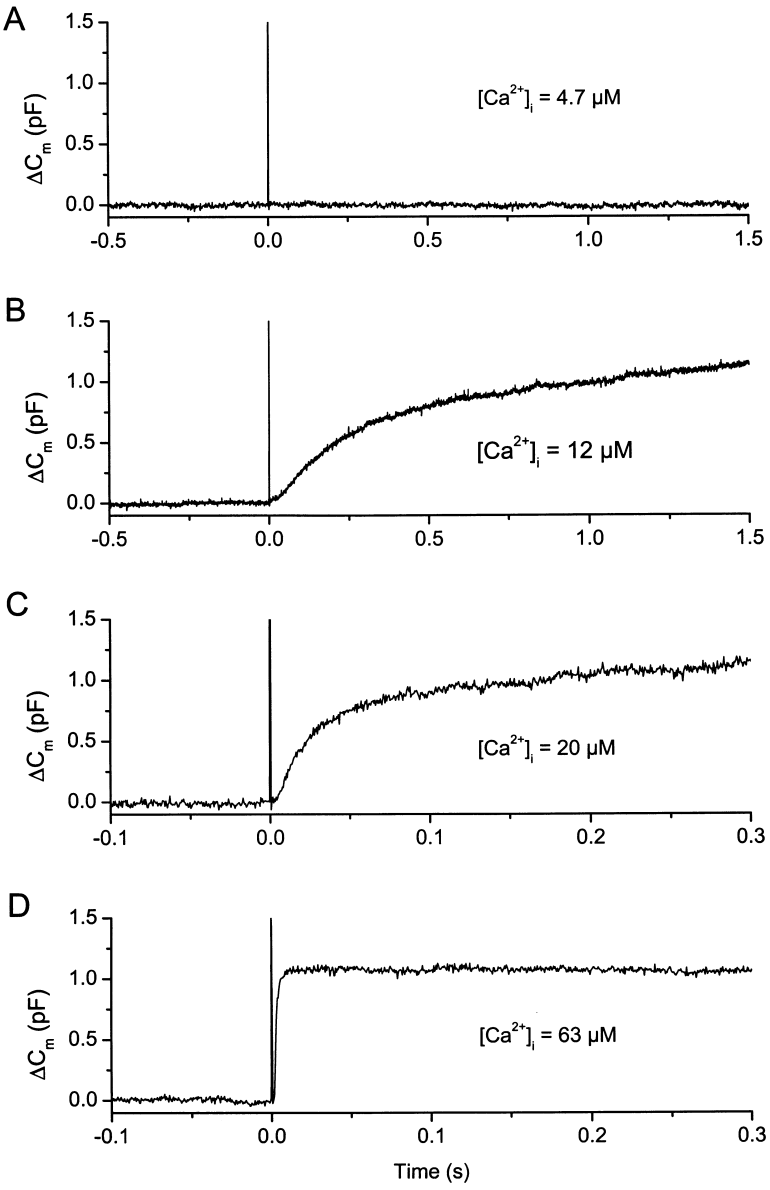

Figure 2. Calcium Dependence of Exocytosis in IHC

(A) Lack of C_m change following $[Ca^{2+}]_i$ increase to 4.7 μM.

(B) A slow C_m change in response to a $[Ca^{2+}]_i$ rise to 12 μM. C_m started to rise after a 4 ms delay with a time constant for the fast exocytic component of ~110 ms.

(C and D) Responses to stronger elevations of $[Ca^{2+}]_i$. The secretory delays (1.5 ms and 0.25 ms, respectively) shortened and the time constants (18 ms and 1.4 ms, respectively) were faster with increasing $[Ca^{2+}]_i$. Note the difference in time scaling between (A) and (B) and (C) and (D).

Peak postflash $[Ca^{2+}]_i$ levels are indicated on each trace.

Using the conversion factor of 37 aF per vesicle (Lenzi et al., 1999), this amplitude corresponds to exocytosis of about 40,000 vesicles. Neither membrane conductance (G_m) nor series conductance (G_s) changed after the flash (Figures 1C and 1D). In some cases, flash-induced alterations of G_m or G_s were observed, but these changes did not correlate temporally or in amplitude with the C_m response.

The inset of Figure 1B shows the first 20 ms of the exocytic response in greater detail. The C_m rise displayed a sigmoidal onset and then followed a double exponential time course. The secretory delay, defined as the time between the Ca^{2+} rise and the interception of the fit with the C_m baseline, was 2.8 ms assuming that 0.4 ms were needed for the Ca^{2+} rise. To transform the C_m increase into release rates, we calculated the first time derivative of the C_m data (dashed line). In this example, a maximal release rate of 132,000 fF/s (3.5×10^6 vesicles/s) was reached 5.1 ms after the Ca^{2+} rise.

Ca^{2+} Dependence of Exocytosis

In our experiments, postflash $[Ca^{2+}]_i$ varied between 4 and 120 μM, despite constant flash intensity and pipette solution composition. This variability is probably due to the intrinsic cell-to-cell variation in basal $[Ca^{2+}]_i$, which causes significant differences in the amount of caged Ca^{2+} that can be released by the flash. Only secretory responses to the first flash were analyzed throughout this study, to avoid bias due to run-down in the absence of MgATP (Heidelberger, 1998). Figure 2 depicts some examples of C_m responses to different flash-induced $[Ca^{2+}]_i$ levels. We failed to detect sizable C_m changes after elevations of $[Ca^{2+}]_i$ to levels below 7 μM (Figure 2A). The time course of the C_m rise in response to larger Ca^{2+} elevations was strongly Ca^{2+} dependent (Figures 2B–2D). The exocytic delay shortened with increasing $[Ca^{2+}]_i$ levels (Figures 2B–2D) and the rate of C_m increase became faster. The total amplitude of the exocytic response did not significantly change with increasing

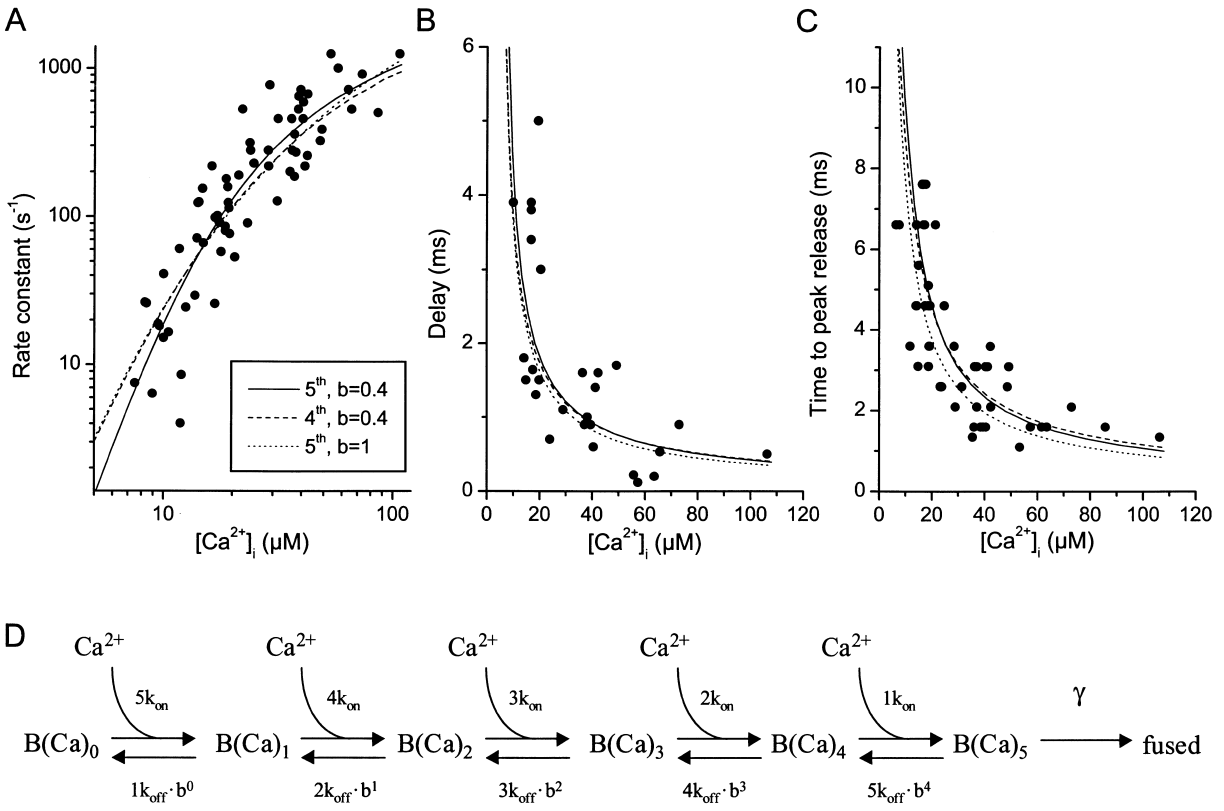

Figure 3. Kinetics of Exocytosis in IHC

(A) Rate constants of the fast component as a function of postflash $[Ca^{2+}]_i$. The rate constant was calculated as the reciprocal of the time constant of the fast component (for details see inset Figure 1).

(B) Exocytic delays versus postflash $[Ca^{2+}]_i$.

(C) Calcium dependence of the time to peak release.

(D) Schematic representation of a kinetic model including a series of five Ca^{2+} binding steps followed by vesicle fusion, which was used for the simulations in Figure 4. For estimation of the parameters, the model was fitted to the Ca^{2+} dependencies of the three kinetic parameters of exocytosis displayed in (A)–(C). The solid line in (A)–(C) represents the best global fit to the experimental data, which yielded the following values: $b = 0.4$, $k_{on} = 27.6\ \mu M^{-1}s^{-1}$, $k_{off} = 2150\ s^{-1}$, and $\gamma = 1695\ s^{-1}$. Best fits with a 5th order model without cooperativity (dotted line) and with a 4th order model with a cooperativity factor of 0.4 (dashed line) are included for comparison.

$[Ca^{2+}]_i$ (mean: 1.52 ± 0.09 pF; n = 68). As an index of the secretory rate, a double exponential function was fitted to the rising phase of each capacitance response (e.g., inset Figure 1B). The fast and the slow component differed in their time constants by approximately one order of magnitude, and the respective contributions of the two components to the total secretory response averaged to 70% and 30%. Following large Ca^{2+} increases, endocytic membrane retrieval was often tightly coupled to exocytosis (see below), complicating the analysis of the slow secretory component. Therefore, the quantitative analysis of the Ca^{2+}-dependent secretion kinetics was restricted to that of the more prominent, fast component.

The rate constant of the fast component of the exocytic response is plotted versus $[Ca^{2+}]_i$ in Figure 3A. It increases over three orders of magnitude between 7 and 40 μM of $[Ca^{2+}]_i$, demonstrating the steep calcium dependence of exocytosis in IHCs. At high $[Ca^{2+}]_i$, fusion of the fast component occurred at rate constants above 1,200 s^{-1}. By multiplying these rate constants with the average number of 28,000 vesicles that fuse during the fast component, we conclude that the maximal rate of exocytosis in IHCs exceeds 3×10^7 vesicles/s at high $[Ca^{2+}]_i$.

It is generally believed that secretory delays reflect the time required for the sequential binding of Ca^{2+} ions to the exocytic machinery. In support of this, we found that increasing $[Ca^{2+}]_i$ levels shortened the secretory delays from the ms to sub-ms range (Figure 3B). Likewise, the time to peak release decreased from 7.5 ms to 1 ms with increasing $[Ca^{2+}]_i$ (Figure 3C).

To quantitatively describe the Ca^{2+}-dependent vesicle fusion, we fitted the kinetic data of Figures 3A–3C with minimal kinetic models, in which a number of sequential and reversible Ca^{2+} binding steps are followed by irreversible vesicle fusion. Fusion schemes involving the binding of four Ca^{2+} ions (dashed lines) or binding of five Ca^{2+} ions without cooperativity (dotted lines) were not able to describe the steep Ca^{2+} dependence of the fusion kinetics for $[Ca^{2+}]_i < 20$ μM. A successful global fit to the data of Figures 3A–3C was obtained with a model in which five cooperative Ca^{2+} binding steps precede an irreversible fusion reaction (Figure 3D). The best global fit (solid lines in Figures 3A–3C) was obtained

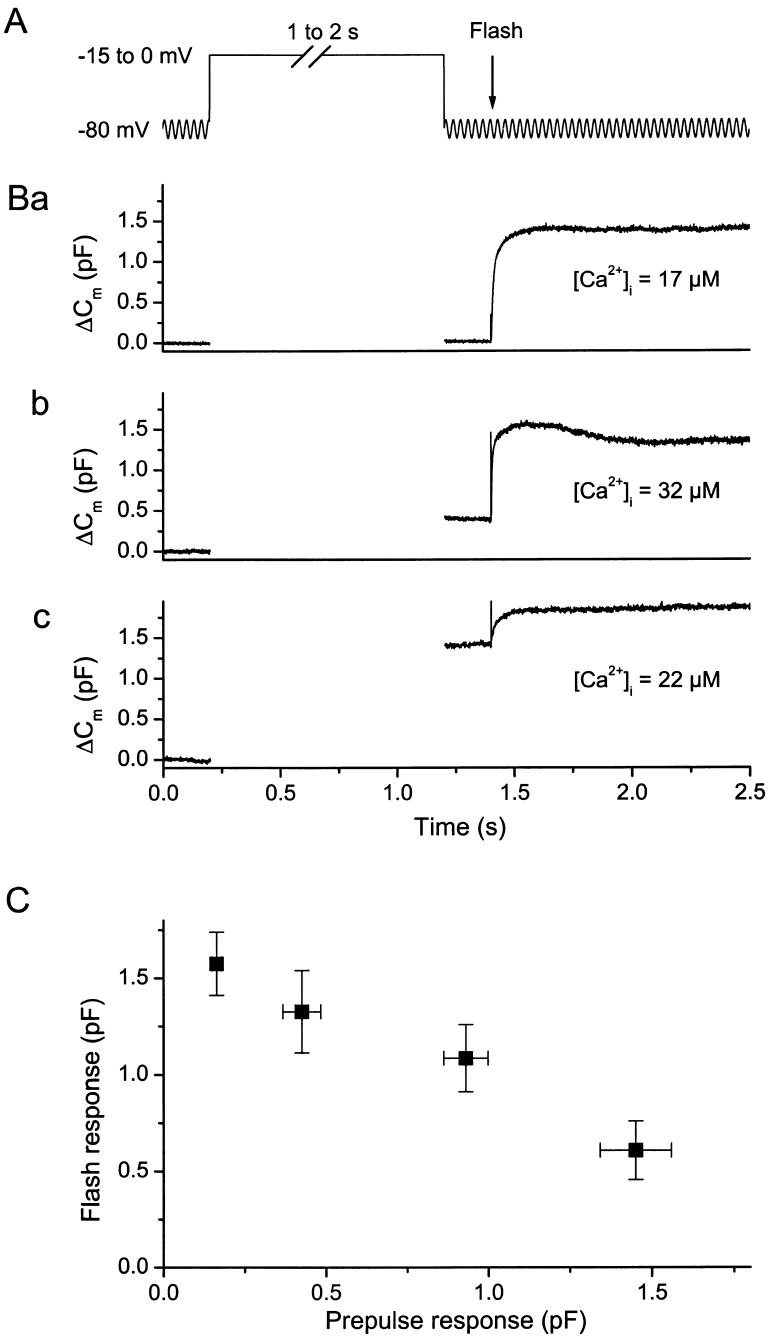

Figure 4. Cross Depletion of Exocytic Responses Triggered by Depolarization and Flash Photolysis

(A) Experimental protocol illustrating the cross depletion paradigm. A flash indicated by the arrow was preceded by a 1–2 s depolarization to potentials between −15 and 0 mV.

(B) Three representative C_m changes from three different cells in response to the experimental protocol shown in (A). In (Ba) and (Bb), the flash was preceded by a 1s depolarization to 0 mV, and in (Bc) by a 1s depolarization to −15 mV. Larger depolarization induced responses correlated with smaller subsequent flash responses. The variability of the depolarization induced responses depended mainly on the variable size of the Ca^{2+} currents.

(C) Analysis of 35 similar experiments. The amplitude of the flash evoked C_m response is plotted against the amplitude of the preceding depolarization induced C_m increase.

with the following values: $k_{on} = 27.6\ \mu M^{-1}s^{-1}$, $k_{off} = 2150\ s^{-1}$, $b = 0.4$, and $\gamma = 1695\ s^{-1}$.

Voltage-Gated Ca^{2+} Influx and Flash Photolysis of Caged Ca^{2+} Trigger Exocytosis from the Same Pool of Vesicles

The physiological stimulus for exocytosis in IHC is voltage-gated Ca^{2+} influx. To investigate whether flash photolysis of caged Ca^{2+} and voltage-gated Ca^{2+} influx recruit vesicles from the same pool, we performed "cross depletion" experiments in which flash photolysis was preceded by 1–2 s depolarizations to voltages between −15 and 0 mV (Figure 4A). Depending on the amplitude and duration of the voltage-gated Ca^{2+} influx, these prepulses caused C_m changes ranging from 100 fF to 1.6 pF. Representative C_m traces illustrate that flash photolysis caused C_m increases that were inversely correlated to the amount of exocytosis triggered by the preceding depolarization (Figure 4B). This is confirmed by results from 35 similar experiments summarized in Figure 4C. Therefore, these data indicate that flash photolysis of caged Ca^{2+} recruits the same pool of vesicles as Ca^{2+} influx through voltage-gated Ca^{2+} channels. Moreover, these results show that the pool of fusion-competent vesicles cannot be fully depleted by depolarizations of up to 2 s.

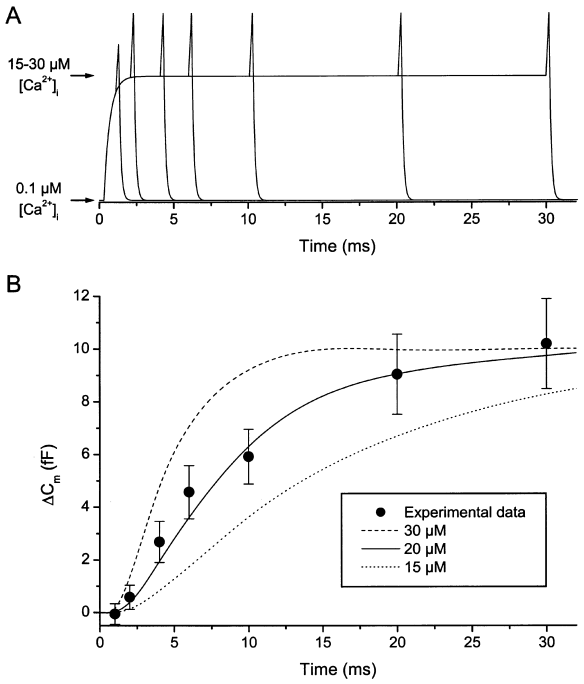

Figure 5. Calcium at Release Sites

(A) Estimated time course of the local $[Ca^{2+}]_i$ signal experienced by readily releasable vesicles at the active zones during depolarizations to −15 mV lasting between 1 and 30 ms. It was assumed that the local $[Ca^{2+}]_i$ signal was proportional to the whole-cell Ca^{2+} current, which had the following characteristics: an activation delay of 0.3 ms, an activation time constant of 0.4 ms, and a deactivation time constant of 0.12 ms, similar to published values (Platzer et al., 2000). (B) The local $[Ca^{2+}]_i$ waveforms shown in (A) and the parameters of the kinetic model (Figure 3D) were used to calculate the time course of fusion of the readily releasable pool (10 fF in size, Moser and Beutner, 2000). Model predictions and experimental data (Figure 4c of Moser and Beutner, 2000, 0.1 mM Ca^{2+}-free EGTA in the pipette solution) matched well when the peak $[Ca^{2+}]_i$ at release sites was between 20 and 30 μM.

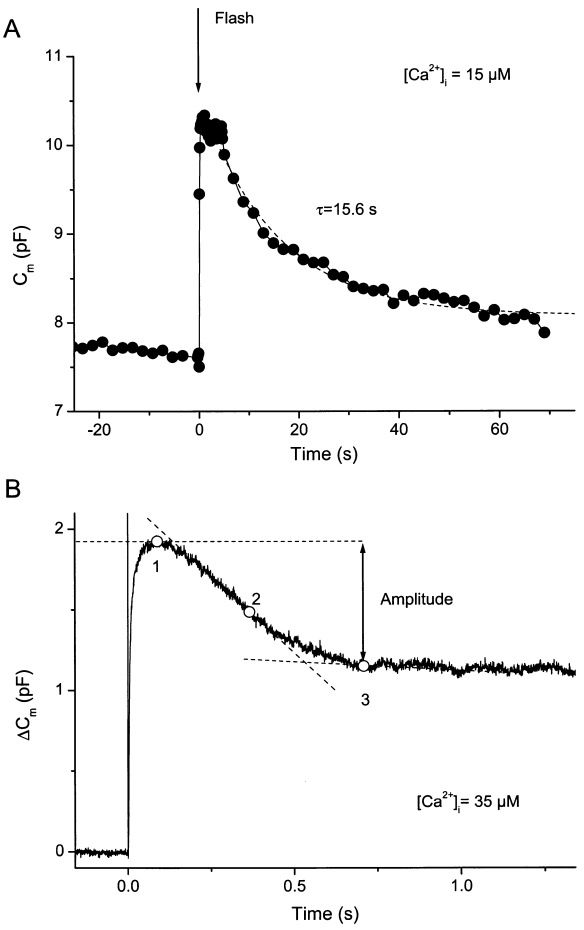

Figure 6. Two Phases of Endocytosis Follow Flash Induced C_m Rise

(A) Example of a flash response followed by slow endocytosis. The timing of the flash is indicated by the arrow. The solid line represents a monoexponential fit to the data yielding a time constant of 15.6 s. (B) Example of a flash response followed by rapid endocytosis. The maximal endocytic rate was determined, after fitting straight lines to overlapping 100 ms segments of the C_m trace, as the maximal negative slope of these lines. In this example the maximal negative slope was reached at point 2. The amplitude of rapid endocytosis was calculated as the C_m difference between the time point where the slope became negative (point 1) and the time point where the endocytic rate decreased to 5% of the maximal rate (point 3). Peak postflash $[Ca^{2+}]_i$ is indicated for both traces.

Calcium at Release Sites

We used the kinetic model introduced in Figure 3D to determine the $[Ca^{2+}]$ concentrations required at the release sites to account for the experimental fusion time course of the readily releasable pool during depolarization to −15 mV (Figure 4c of Moser and Beutner, 2000). The time course of the $[Ca^{2+}]$ sensed by the exocytic machinery was assumed to mimic that of the whole-cell Ca^{2+} current measured in IHCs. This is a valid approximation when Ca^{2+} at release sites is governed by Ca^{2+} influx through several neighboring Ca^{2+} channels (Roberts et al., 1990). The resulting Ca^{2+} waveforms (Figure 5A) were scaled to reach different peak $[Ca^{2+}]_i$ levels and used to drive the theoretical model of Figure 3D. We found that $[Ca^{2+}]_i$ levels at the release sites in the range of 20–30 μM were sufficient to reproduce the experimentally observed fusion rate (Figure 5B).

Calcium Dependence of Rapid Endocytosis

After a flash, the membrane added by exocytosis was in general fully retrieved. We observed two distinct kinetic components in the time course of endocytosis. At $[Ca^{2+}]_i$ levels below 15 μM, the time course of endocytosis was in most cases well approximated by a single exponential with an average time constant of 16.6 ± 2.4 s (n = 13; Figure 6A). Higher postflash $[Ca^{2+}]_i$ levels additionally activated a second and much faster type of endocytosis, which retrieved a significant fraction of the exocytosed membrane within one second (Figure 6B). We quantified the maximal rate and the amplitude of rapid endocytosis as illustrated in Figure 6B. Rapid endocytosis was defined as retrieval of more than 5% of the previously exocytosed membrane within 1 s. The percentage of cells that exhibited rapid endocytosis increased from about 15% at 15 μM $[Ca^{2+}]_i$ to more than 90% when $[Ca^{2+}]_i$ was higher than 40 μM. In cells showing rapid endocytosis higher $[Ca^{2+}]_i$ levels also increased the fraction of membrane retrieved by this mechanism. Figure 7A plots the percentage of previously exocytosed mem-

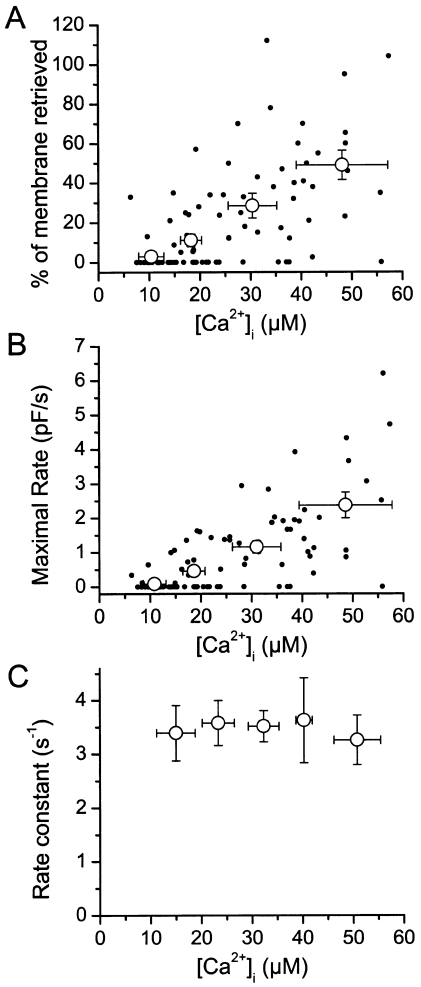

Figure 7. Calcium Dependence of Rapid Endocytosis

(A) Percentage of flash induced exocytosed membrane that is retrieved within one second as a function of peak postflash $[Ca^{2+}]_i$. Data points represent the results of 93 cells. For cells that did not retrieve 5% of the previously added membrane within one second, the amplitude was set to 0%.

(B) Maximal rate (pF/s) of membrane retrieval versus peak postflash $[Ca^{2+}]_i$.

(C) Rate constant (s^{-1}) of rapid endocytosis as a function of peak postflash $[Ca^{2+}]_i$ from 55 cells that met the 5% criterion. Rate constants were obtained by dividing the maximal endocytic rate by the amplitude of rapid endocytosis.

brane retrieved by rapid endocytosis versus postflash $[Ca^{2+}]_i$. Each data point represents the result from a single cell. For cells not qualifying for the rapid endocytosis criterion the amplitude was set to 0%. Excess endocytosis, whereby the amount of rapidly retrieved membrane exceeds the preceding exocytosis (Henkel and Almers, 1996; Smith and Neher, 1997; Engisch and Nowycky, 1998), was only observed in two out of 86 cells. Higher $[Ca^{2+}]_i$ levels increased the maximal rate of rapid endocytosis (Figure 7B). However, the rate constant of rapid endocytosis, which was obtained by dividing the maximal rate by the amplitude, was found to be $\sim$3.5 s^{-1} and independent of $[Ca^{2+}]_i$ (Figure 7C). These results indicate that $[Ca^{2+}]_i$ determines the onset and extent of rapid endocytosis but does not influence its kinetics.

Discussion

In this study we have combined Ca^{2+} uncaging with membrane capacitance measurements to investigate the Ca^{2+} dependence of exo- and endocytosis in a mature presynaptic preparation from mouse. Using these methods we revealed several properties that may underlie the ability of these sensory cells to produce both rapid and sustained phases of transmitter release. These properties include a steep Ca^{2+} dependence of vesicle fusion, a large reservoir of fusion competent vesicles, and two complementary modes of endocytosis that ensure efficient membrane retrieval under various stimulus intensities.

Ca^{2+} Dependence of Exocytosis

Experiments combining flash photolysis of caged Ca^{2+} and membrane capacitance measurements have been previously used to determine the Ca^{2+} dependence of the rate of vesicle fusion in a number of neurosecretory preparations. In retinal bipolar cells, little exocytosis occurred at $[Ca^{2+}]_i$ levels below 20 μM, and $[Ca^{2+}]_i$ levels of more than 100 μM at release sites were required to produce the high rates of secretion observed during electrical stimulation (Heidelberger et al., 1994; Mennerick and Matthews, 1996). In contrast, studies in chromaffin cells (Heinemann et al., 1994; Voets, 2000) and in the calyx of Held glutamatergic synapse (Bollmann et al., 2000; Schneggenburger and Neher, 2000) showed already measurable release at sub-micromolar to low micromolar $[Ca^{2+}]_i$. Our present results indicate that the Ca^{2+} dependence of release in IHCs is closer to the relatively high affinity reported for chromaffin cells and the calyx of Held. For $[Ca^{2+}]_i$ levels between 10 and 100 μM, we observed exocytic rate constants that were 5 to 10 times higher than for the bipolar cells. We calculated that during electrical stimulation, $[Ca^{2+}]$ at the release sites does not need to exceed 20–30 μM, similar to findings in chromaffin cells (Chow et al., 1994; Voets et al., 1999) and the calyx of Held (Bollmann et al., 2000; Schneggenburger and Neher, 2000). However, in contrast to the latter preparations, we did not observe any exocytic activity for $[Ca^{2+}]_i$ below 7 μM. Unfortunately, we cannot exclude that low rates of release at these moderate $[Ca^{2+}]_i$ levels remained undetected by our C_m measurements, because this technique is not sensitive enough to resolve the fusion of single synaptic vesicles (37 aF, Lenzi et al., 1999). In this context, it should be noted that exocytic rates of up to 2000 vesicles/s at $[Ca^{2+}]_i$ below 1 μM have been measured by FM 1-43 fluorescence in retinal bipolar cells (Lagnado et al., 1996), which may have missed detection in the capacitance measurements by Heidelberger et al. (1994).

At present, it remains unclear what causes the considerable quantitative differences in the Ca^{2+} dependence of release observed between various neurosecretory preparations. Presumably, different cell types utilize Ca^{2+}-sensing molecules with different Ca^{2+} affinities to trigger exocytosis. In this context, it is important to note that Synaptotagmins I and II, which have been proposed

as the major Ca^{2+} sensors for synchronous and asynchronous release in the brain (Geppert et al., 1994), are not expressed to detectable levels in the cochlea (Safieddine and Wenthold, 1999). Therefore, rapid exocytosis in IHCs seems not to depend on Synaptotagmin I-II.

Flash Photolysis Triggers Exocytosis of a Large Pool of Fusion-Competent Vesicles in IHCs

The average C_m increases in response to single flashes corresponded to the fusion of a pool of ~40,000 vesicles. At the highest $[Ca^{2+}]_i$ levels tested, this C_m increase was completed within a few milliseconds, indicating that these vesicles were all fusion competent. Our estimate of the amount of fusion competent vesicles in IHCs exceeds estimates in other presynaptic terminals (e.g., 1000 in retinal bipolar neurons [Heidelberger et al., 1994] and ~2000 in the calyx of Held [Schneggenburger and Neher, 2000]) by more than one order of magnitude. These results also indicate that the amount of fusion-competent vesicles largely outnumbers the pool of readily releasable vesicles that are docked at the active zones of IHCs in close vicinity to Ca^{2+} channels (300, see Moser and Beutner, 2000). Moreover, our cross-depletion experiments demonstrate that this large pool of fusion-competent vesicles is only partially depleted by depolarizations of up to 1–2 s. We therefore conclude that the exocytosis of fusion-competent vesicles at some distance from the Ca^{2+} channels at the active zones largely contributes to the slower, sustained phase of release during prolonged stimulation (Parsons et al., 1994; Moser and Beutner, 2000). The slower release of these vesicles most likely reflects the lower $[Ca^{2+}]_i$ signal that these vesicles experience due to the increased distance from Ca^{2+} channels.

The occurrence of vesicle fusion outside active zones has also been shown in recent studies using light- and electronmicroscopical techniques. Lenzi et al. (1999) presented electronmicrographs of frog saccular hair cells showing synaptic vesicles docked to the presynaptic membrane at some distance from active zones. Using total internal reflection microscopy in retinal bipolar nerve terminals, Zenisek et al. (2000) observed fusion events outside the zones of highest fusion activity and proposed that these "outliers" correspond to the fusion of vesicles outside the ribbon-type active zones. However, the extent to which the release of vesicles outside active zones actually contributes to synaptic transmission in these different systems remains to be examined.

Endocytosis in IHCs Involves Two Kinetically Distinct Types of Membrane Retrieval

Endocytic retrieval of exocytosed membrane is a fundamental process for maintaining a neuron's secretory response and plasma membrane homeostasis (for review, see Henkel and Almers, 1996). However, the factors that regulate endocytosis and in particular the role of cytosolic Ca^{2+} are not well understood and remain highly controversial. For example, high $[Ca^{2+}]_i$ levels appear to activate a rapid mode of endocytosis in hippocampal neurons and adrenal chromaffin cells (Neher and Zucker, 1993; Artalejo et al., 1995; Smith and Neher, 1997; Klingauf et al., 1998). In contrast, endocytosis was reported to be independent of $[Ca^{2+}]_i$ at the frog neuromuscular junction (Wu and Betz, 1996) and even inhibited by high $[Ca^{2+}]_i$ in bipolar nerve terminals (von Gersdorff and Matthews, 1994).

In this study, we present evidence for a scenario in which $[Ca^{2+}]_i$ regulates endocytosis in IHCs by determining the relative contribution of two kinetically distinct modes of membrane retrieval. We mostly found a monoexponential time course of endocytosis ($\tau \approx 15$ s) when postflash $[Ca^{2+}]_i$ was below ~15 μM, slightly slower than endocytosis following short depolarizations (mean time constants of 7.5 s, see Moser and Beutner, 2000). Higher $[Ca^{2+}]_i$ levels did not appear to affect the time constant of this slow endocytic mode but, instead, caused the gradual activation of a second, much faster ($\tau \approx 300$ ms) mode of endocytosis, which became dominant at the highest $[Ca^{2+}]_i$ levels tested. It thus appears that each exocytosed vesicle can be retrieved by two distinct endocytic mechanisms, and that Ca^{2+} increases the probability of a vesicle being endocytosed by the fast mode. Activation of the rapid endocytic mode when stimulus intensity is high may be advantageous in achieving sufficient vesicle recycling, thereby contributing to the ability of IHCs to maintain accurate information transfer during prolonged sound stimuli. Such a Ca^{2+}-dependent switch between rapid and slow modes of endocytosis may represent a general mechanism whereby synapses adapt the rate of membrane retrieval to the level of stimulation.

Conclusions

Our present results indicate that depolarization-evoked phasic release originates from a small fraction of the total pool of fusion-competent vesicles that are docked at the active zones in close vicinity to Ca^{2+} channels. The sustained component of release most likely involves both vesicle fusion outside of the active zones and rapid recruitment of vesicles to the active zones (Moser and Beutner, 2000). We suggest that these properties in conjunction with efficient mechanisms of membrane retrieval fulfill the requirements for efficient signal transduction at the IHC afferent synapse.

Experimental Procedures

Whole-Cell Recordings

IHCs from the apical coil of freshly dissected semi-intact organs of Corti from hearing mice (Naval Medical Research Institute, postnatal days 14 through 25) were used for experiments. The isolated cochleae were dissected and the organ of Corti was separated from the stria vascularis and most of the modiolus. The tectorial membrane and neighboring supporting cells were removed with a cleaning pipette before the patch pipette was sealed onto the basolateral membrane of an IHC. Pipette solutions contained (in mM): 120 Cs-gluconate, 20 TEA-Cl, 20 CsOH-HEPES, 10 DM-nitrophen, 10 $CaCl_2$, 5 DPTA, and 1 Furaptra (pH 7.2). Mg^{2+}-ATP was not included in the internal solution to avoid complications arising from the binding of Mg^{2+} to DM-nitrophen and furaptra as well as to slow down the action of the Ca^{2+} ATPases in IHCs. Control experiments using a pipette solution containing (in mM) 110 Cs-glutamate, 8 NaCl, 2 Mg-ATP, 0.3 Na_2-GTP, 20 CsOH-HEPES, 4 $CaCl_2$, 1 Furaptra, and 5 nitrophenyl-EGTA as photolyzable Ca^{2+} chelator revealed that neither Mg^{2+} nor ATP had any significant influence on the kinetics of exocytosis. The recording chamber was perfused at a flow rate of 1–2 ml/min with extracellular solution containing (in mM): 105 NaCl, 35 TEA-Cl, 2.8 KCl, 1 $MgCl_2$, 10 NaOH-HEPES, 10 D-glucose and 10 $CaCl_2$ (pH 7.2). Conventional whole-cell recordings (Hamill et al., 1981) were performed with 3–4 MΩ sylgard™ coated pipettes. All experiments were performed at room temperature (20°C–25°C). Se-

ries resistances ranged from 4–17 MΩ. An EPC-9 amplifier (HEKA-electronics, Lambrecht, Germany) controlled by "Pulse"-software (HEKA) was used for measurements. All voltages were corrected for liquid junction potentials (−10 mV).

Capacitance Measurements

We measured C_m using the Lindau-Neher technique (Lindau and Neher, 1988) implemented in the software-lockin module of Pulse combined with compensation of pipette and resting cell capacitance by the EPC-9 compensation circuitry's. A 2 kHz, 70 mV peak to peak sinusoid was applied around a DC holding potential of −80 mV. Data were acquired through a combination of the high time resolution PULSE software and the lower time resolution X–Chart plug-in module to the PULSE software.

Photolysis of Caged Calcium and Measurement of $[Ca^{2+}]_i$

To obtain step-wise increases in $[Ca^{2+}]_i$, short (1.3 ms) flashes of ultraviolet light from a Xenon arc flash lamp (Rapp OptoElectronics, Hamburg, Germany) were applied to the whole cell. $[Ca^{2+}]_i$ was measured by dual-wavelength ratiometric fluorimetry with the indicator dye Furaptra. The dye was excited with light alternating between 350 and 380 nm using a monochromator-illumination based system (TILL photonics, Martinsried, Germany), and the resulting fluorescent signal was measured using a photomultiplier. $[Ca^{2+}]_i$ was determined from the ratio R of the fluorescent signals at both wavelength according to

$$[Ca^{2+}]_i = K_{eff}\frac{R - R_{min}}{R_{max} - R}$$

where R_{min} and R_{max} are calibration constants obtained from in vivo calibration. K_{eff} was calculated according to

$$K_{eff} = K_D\frac{R_{max} + \alpha}{R_{min} + \alpha}$$

where K_D, the dissociation constant of furaptra, equals 31 μM, as measured in vitro when dissolved at 1 mM in pipette solution. The isocoefficient, α (Zhou and Neher, 1993), was measured to be 0.1. The monochromator light was not only used to measure $[Ca^{2+}]_i$ but also helped to sustain $[Ca^{2+}]_i$ after a flash by photolyzing additional small amounts of DM-nitrophen.

Analysis and Numerical Calculations

All experimental data were first analyzed with the program IgorPro 3.12 (Wavemetrics, Lake Oswego, OR) and then transferred to Origin 6.0 (Microcal Software, Northampton, MA) for further statistical analysis and display. Averaged data are expressed as mean ± SE.

The differential equations describing the vesicle fusion kinetics were solved using a fifth-order Runge-Kutta integration scheme with adaptive step size. The downhill simplex method was used to find parameters that gave the best fit to the experimental results.

Acknowledgments

We would like to thank S. Pyott and R. Schneggenburger for critical feedback on the manuscript and M. Pilot for excellent technical assistance. T. V. is a postdoctoral fellow of the Fund for Scientific Research, Flanders (FWO-Vlaanderen). This work was supported by a grant from the Deutsche Forschungsgemeinschaft to T. M. (MO 896/1).

Received November 20, 2000; revised January 24, 2001.

References

Artalejo, C.R., Henley, J.R., McNiven, M.A., and Palfrey, H.C. (1995). Rapid endocytosis coupled to exocytosis in adrenal chromaffin cells involves Ca2+, GTP, and dynamin but not clathrin. Proc. Natl. Acad. Sci. USA *92*, 8328–8332.

Bollmann, J.H., Sakmann, B., and Borst, J.G. (2000). Calcium sensitivity of glutamate release in a calyx-type terminal. Science *289*, 953–957.

Chow, R.H., Klingauf, J., and Neher, E. (1994). Time course of Ca2+ concentration triggering exocytosis in neuroendocrine cells. Proc. Natl. Acad. Sci. USA *91*, 12765–12769.

Engisch, K.L., and Nowycky, M.C. (1998). Compensatory and excess retrieval: two types of endocytosis following single step depolarizations in bovine adrenal chromaffin cells. J. Physiol. *506*, 591–608.

Geppert, M., Goda, Y., Hammer, R.E., Li, C., Rosahl, T.W., Stevens, C.F., and Sudhof, T.C. (1994). Synaptotagmin I: a major Ca2+ sensor for transmitter release at a central synapse. Cell *79*, 717–727.

Gomis, A., Burrone, J., and Lagnado, L. (1999). Two actions of calcium regulate the supply of releasable vesicles at the ribbon synapse of retinal bipolar cells. J. Neurosci. *19*, 6309–6317.

Hamill, O.P., Marty, A., Neher, E., Sakmann, B., and Sigworth, F.J. (1981). Improved patch-clamp techniques for high-resolution current recording from cells and cell-free membrane patches. Pflügers Arch. *391*, 85–100.

Heidelberger, R. (1998). Adenosine triphosphate and the late steps in calcium-dependent exocytosis at a ribbon synapse. J. Gen. Physiol. *111*, 225–241.

Heidelberger, R., Heinemann, C., Neher, E., and Matthews, G. (1994). Calcium dependence of the rate of exocytosis in a synaptic terminal. Nature *371*, 513–515.

Heinemann, C., Chow, R.H., Neher, E., and Zucker, R.S. (1994). Kinetics of the secretory response in bovine chromaffin cells following flash photolysis of caged Ca2+. Biophys. J. *67*, 2546–2557.

Henkel, A.W., and Almers, W. (1996). Fast steps in exocytosis and endocytosis studied by capacitance measurements in endocrine cells. Curr. Opin. Neurobiol. *6*, 350–357.

Kaplan, J.H., and Ellis-Davies, G.C. (1988). Photolabile chelators for the rapid photorelease of divalent cations. Proc. Natl. Acad. Sci. USA *85*, 6571–6575.

Kiang, N.Y.-S., Watanabe, T., Thomas, E.C., and Clark, L.F. (1965). Discharge pattern of single fibers in the cat's auditory nerve. Research Monograph No. 35 Edition (Cambridge, MA: MIT Press).

Klingauf, J., Kavalali, E.T., and Tsien, R.W. (1998). Kinetics and regulation of fast endocytosis at hippocampal synapses. Nature *394*, 581–585.

Konishi, M., Hollingworth, S., Harkins, A.B., and Baylor, S.M. (1991). Myoplasmic calcium transients in intact frog skeletal muscle fibers monitored with the fluorescent indicator furaptra. J. Gen. Physiol. *97*, 271–301.

Lagnado, L., Gomis, A., and Job, C. (1996). Continuous vesicle cycling in the synaptic terminal of retinal bipolar cells. Neuron *17*, 957–967.

Lenzi, D., Runyeon, J.W., Crum, J., Ellisman, M.H., and Roberts, W.M. (1999). Synaptic vesicle populations in saccular hair cells reconstructed by electron tomography. J. Neurosci. *19*, 119–132.

Lindau, M., and Neher, E. (1988). Patch-clamp techniques for time-resolved capacitance measurements in single cells. Pflügers Arch. *411*, 137–146.

Matthews, G. (2000). Vesicle fiesta at the synapse. Nature *406*, 835–836.

Mennerick, S., and Matthews, G. (1996). Ultrafast exocytosis elicited by calcium current in synaptic terminals of retinal bipolar neurons. Neuron *17*, 1241–1249.

Moser, T., and Beutner, D. (2000). Kinetics of exocytosis and endocytosis at the cochlear inner hair cell afferent synapse of the mouse. Proc. Natl. Acad. Sci. USA *97*, 883–888.

Neher, E., and Zucker, R.S. (1993). Multiple calcium-dependent processes related to secretion in bovine chromaffin cells. Neuron *10*, 21–30.

Parsons, T.D., Lenzi, D., Almers, W., and Roberts, W.M. (1994). Calcium-triggered exocytosis and endocytosis in an isolated presynaptic cell: capacitance measurements in saccular hair cells. Neuron *13*, 875–883.

Platzer, J., Engel, J., Schrott-Fischer, A., Stephan, K., Bova, S., Chen, H., Zheng, H., and Striessnig, J. (2000). Congenital deafness and sinoatrial node dysfunction in mice lacking class D L-type Ca2+ channels. Cell *102*, 89–97.

Roberts, W.M., Jacobs, R.A., and Hudspeth, A.J. (1990). Colocalization of ion channels involved in frequency selectivity and synaptic transmission at presynaptic active zones of hair cells. J. Neurosci. *10*, 3664–3684.

Safieddine, S., and Wenthold, R.J. (1999). SNARE complex at the ribbon synapses of cochlear hair cells: analysis of synaptic vesicle- and synaptic membrane-associated proteins. Eur. J. Neurosci. *11*, 803–812.

Schneggenburger, R., and Neher, E. (2000). Intracellular calcium dependence of transmitter release rates at a fast central synapse. Nature *406*, 889–893.

Sewell, W.F. (1996). Physiology of mammalian cochlea hair cells. In The Cochlea, P. Dallos, A.N. Popper and R.R. Fay, eds. (New York: Springer), pp. 503–532.

Smith, C., and Neher, E. (1997). Multiple forms of endocytosis in bovine adrenal chromaffin cells. J. Cell Biol. *139*, 885–894.

Smith, C.A., and Sjostrand, F.S. (1961). A synaptic structure in the hair cells of the guinea pig cochlea. J. Ultrastruct. Res. *5*, 184–192.

Voets, T. (2000). Dissection of three Ca2+-dependent steps leading to secretion in chromaffin cells from mouse adrenal slices. Neuron *28*, 537–545.

Voets, T., Neher, E., and Moser, T. (1999). Mechanisms underlying phasic and sustained secretion in chromaffin cells from mouse adrenal slices. Neuron *23*, 607–615.

von Gersdorff, H., and Matthews, G. (1994). Inhibition of endocytosis by elevated internal calcium in a synaptic terminal. Nature *370*, 652–655.

von Gersdorff, H., Vardi, E., Matthews, G., and Sterling, P. (1996). Evidence that vesicles on the synaptic ribbon of retinal bipolar neurons can be rapidly released. Neuron *16*, 1221–1227.

Wu, L.G., and Betz, W.J. (1996). Nerve activity but not intracellular calcium determines the time course of endocytosis at the frog neuromuscular junction. Neuron *17*, 769–779.

Zenisek, D., Steyer, J.A., and Almers, W. (2000). Transport, capture and exocytosis of single synaptic vesicles at active zones. Nature *406*, 849–854.

Zhou, Z., and Neher, E. (1993). Mobile and immobile calcium buffers in bovine adrenal chromaffin cells. J. Physiol. *469*, 245–273.